Engineering and Technology Journal
Journal homepage: https://etj.uotechnology.edu.iq

Effect of Cordierite Additions on Mechanical Properties of Hydroxyapatite Used in Medical Applications

Zainab J.Kadhim*, Fatimah J. Al-hasani, Emad S. Al-hassani

Materials Engineering Dept., University of Technology-Iraq, Alsina'a street, 10066 Baghdad, Iraq.
*Corresponding author Email:mae.20.72@grad.uotechnology.edu.iq

HIGHLIGHTS

- The incorporationof cordierite caused a slight increase in grain size at all sintering temperatures.
- At 1100°C, 30% cordierite increased the compressive strength of HA by 116.23% at 700°C, 57.80% at 900°C, and 94.34 % at 1100°C.
- The effect of the cordierite on hardness was increased by 6.09% at 700 °C, 108.71% at 900°C, and 66.59 % at 1100 °C.

ARTICLE INFO

Handling editor: Mustafa H. Al-Furaiji

Keywords:

Cordierite
Hydroxyapatite
Ceramic-composite
Bone grafting
Mechanical properties

ABSTRACT

In this study, a novel bioceramic material with improved mechanical properties was prepared to be consentient with the mechanical requirements of living bodies. Cordierite was synthesized via the sintering method at 1400°C, based on a composition of 51.4% silica, 34.8% of alumina, and 13.8% magnesia. The composition of precursor materials was studied using wet chemical analysis. Three different compositions of the cordierite (30, 40, and 50 wt.%) were incorporated in hydroxyapatite and then sintered at 700, 900, and 1100°C. To visualize the characteristics of all prepared materials, scanning electron microscopy (SEM) and X-ray diffraction (XRD) were analyzed. The crystallite size was determined from XRD patterns using the Scherrer equation. Microhardness was investigated using (a digital micro hardness tester), while the compressive strength was tested using a microcomputer-controlled electronic universal testing machine (WDW-5E). The modulus of elasticity was determined from the stress-strain curve. As a result, all samples which contain cordierite powder have considerable mechanical properties as compared to the control sample. The incorporation of cordierite caused a slight increase in grain size at all sintering temperatures. Among all ratios, the second mixture, which includes 40% cordierite showed the best mechanical properties at all sintering temperatures. The percentage of 40% cordierite led to increasing the compressive strength of HA by 126.27% at 700°C, 61.52% at 900°C, and 123.05% at 1100 °C. On the other hand, the effect of this cordierite level on hardness increased by 94.04% at 700°C, 141.29% at 900°C, and 128.44% at 1100°C. The values of elasticity modulus ranged between 15-37 GPa, i.e. consistent with that of cortical bone.

1. Introduction

Hydroxyapatite (AH), also known as calcium phosphate, has the chemical formula $Ca_{10}(PO_4)_6(OH)_2$ and is a bioceramic material that is frequently used for hard tissue regeneration due to its excellent biocompatibility, high osteoconductivity, and chemical similarity to biological apatite found in human hard tissues [1]. However, the mechanical characteristics of HA bioceramics are much lower than those of human bone. Thus, in spite of its better biological activity, the mechanical properties of HA bioceramics are significantly limit its clinical uses, such as prosthetic teeth and bones[2]. In addition, it is barely degradable, preventing full bone replacement and remodeling and severely limiting their clinical applicability. As a result, there is a need to improve the mechanical characteristics and degradability of HA-based bioceramics. Until recently, developing composite materials was one of the most frequent strategies for manipulating material characteristics.

In the most recent decades, hydroxyapatite (HA)-based composites have been widely inspected with particular attention to investigate physical, mechanical, and biocompatibility characteristics of HA in the existence of other second compounds. Until now, HA-Al_2O_3, AH-ZrO_2, and HA-bioglass composites are well studied as much as their mechanical properties are concerned.Hossan et al. composited gelatin with hydroxyapatite to prepare a scaffold that mimics the natural bone with improved mechanical properties. The resulting material exhibited Vickers hardness larger than 200 Hv and it possesses biodegradability and biocompatibility making it suitable as bone substitute material [3]. Majid et al used HA/Al_2O_3 with three

http://doi.org/10.30684/etj.2023.138142.1375
Received 03 February 2023; Accepted 04 April 2023; Available online 12 May 2023
2412-0758/University of Technology-Iraq, Baghdad, Iraq

different percentages of alumina to improve the flexural strength, impact strength, surface hardness, and shrinkage behavior of PMMA. Flexural strength increased by 35% as compared to pure PMMA. Also, impact strength was 2.5 times of these control PMMA, and Vickers hardness increased by 10% more than neat PMMA[4].

Eclan et. al used different concentrations (0-5wt%) of ZrO_2 to estimate the mechanical properties of hydroxyapatite at lower temperatures using microwave sintering. As a result, they found that 700 °C insufficient to cause densification of the prepared material. The temperature of 1200 °C produced the dense bodies, and increasing ZrO_2 pins the grain boundaries [5]. Baradaran et. al used nano graphene oxide to reinforce nano-hydroxyapatite to produce (nHA/nGO) composite in order to overcome the limitations and disadvantages of HA and improve mechanical and biological performance. Results showed that elastic modulus and fracture toughness increased by 86% and 40% respectively [6].

In the work of Mohammad et. al, bioactive glass (20 wt%) was used to strengthen hydroxyapatite, and the effect of different synthesis processes on the morphological and microstructural properties of hydroxyapatite-bioactive glass composite prepared by sol-gel method was investigated. The results showed that crystallite size, crystallinity, shape, and specific surface area were largely dependent on the process and technique of synthesis [7]. Xiuyong et al studied the mechanical properties of nano diamond-reinforced HA composite coatings deposited on titanium substrate using plasma spray. They found that the composite coating reduced apparent porosity and exhibit uniform microstructure. Consequently, mechanical properties were enhanced in comparison to the control sample [8].

Chen et al. used gelatin, chitosan, and carboxymethyl with hydroxyapatite to prepare composite scaffolds with improved properties via a 3D printing approach. They found that the maximum compressive strength was 14.3 MPa after optimizing the microstructure [9]. Ping et al, was prepared a hybrid composite scaffold with improved mechanical and biological properties via bioinspired fabrication. The highest mechanical strength achieved was 9.41 ±1.63 MPa and the elastic modulus was 0,17±0.02 GPa [10]. Ziquan et al used magnesium oxide and mineralized hydroxyapatite to fabricate a 3D silk fibroin scaffold for bone regeneration. They found that the addition of MgO and mineralized HA made the scaffold have superior physical and chemical characteristics, and cell and osteogenic activity. The maximum compressive strength achieved was 7.11±1.69 MPa [11]. Maksym et. al had been used a multi-walled carbon nanotube to improve the properties of HA. The results showed increasing the Vickers hardness by 1.3 times, elasticity index by 1.5 times, and resistance to plastic deformation by ~ 3 times[12].

Many researchers focused on the use of cordierite as biocompatible material to prepare highly porous scaffolds. Marzieh et. al prepared cordierite by Pechini method to evaluate its effect in the PU matrix. The results showed that by incorporating cordierite into the polymer up to 2wt. %, the NLR index increased. The thermal effect is responsible for nonlinearity in this section [13]. Hamisah et. al used cordierite and wollastonite, by (50/50 wt.%), to prepare a novel bioactive ceramic composite used to regenerate bone tissues. They found that pure cordierite is bioinert ceramic and doesn't cause the formation of an apatite-like layer. The addition of wollastonite showed a good influence on the bioactivity of cordierite during immersion in SBF [14]. Recently, we have developed another new combination of HA-based material with Cordierite ($5SiO_2.2Al_2O_3.2MgO$) as a reinforcing phase.

Cordierite is a naturally occurring magnesium aluminum silicate ceramic material that includes 51.4% of silicon oxide, 34.8% of aluminum oxide, and 13.8% magnesium oxide with the chemical formula of $Mg_2Al_4Si_5O_{18}$[15]. Cordierite comes in two varieties: natural and synthetic. Cordierite crystallizes in two polymorphic forms in nature: an orthorhombic low-temperature form and a hexagonal high-temperature form. Low cordierite is converted to high cordierite by high-temperature heat treatment, whereas high cordierite is never converted to low cordierite. Cordierite crystallizes synthetically in three polymorphic forms: (high-temperature phase), (low-temperature form), and (meta-stable state) [15,16]. They have varied optical characteristics and are hexagonal crystal structures (cyclosilicate sheets). Synthetic cordierite possesses several features, including a low dielectric constant, a low dielectric loss, a low thermal expansion, a high chemical durability, a low thermal conductivity, and a high hardness (7-7.5 on the Moh's scale) [15].

In this work, we prepared Hydroxyapatite/cordierite powder via a powder sintering technique to estimate the effect of cordierite on the mechanical properties of hydroxyapatite. To our knowledge, the preparation of Cordierite/Hydroxyapatite powder via a powder sintering technique has not yet been reported. In the present paper, we focus on the use of three weight percent of cordierite e.g. (30, 40, and 50 wt.%), and sintered at three different sintering temperatures (700 °C, 900 °C, and 1100°C). From the literature, it is reported that the highest compressive strength was 14.3 MPa after optimizing the microstructure [9]. In another study,the maximum mechanical strength achieved was 9.41 ±1.63 MPa and the elastic modulus was 0.17±0.02 GPa [10]. In the study of Ziquan et al, the maximum compressive strength achieved was 7.11±1.69 MPa using magnesium oxide and mineralized hydroxyapatite to fabricate a 3D silk fibroin scaffold for bone regeneration [11].

In the work of Hossan et al, the resulting material exhibited Vickers hardness larger than 200 Hv (~1.9 GPa) and it possesses biodegradability and biocompatibility making it suitable as bone substitute material [3]. As compared with previous studies, our highest compressive strength, hardness, and elasticity modulus were higher than 50 MPa, 9 GPa, and 36 GPa respectively.

2. Experimental Work

2.1 Synthesis of Cordierite Ceramic Nano Powder

Cordierite was prepared via a solid-state process based on a stoichiometric mixture of 51.4% SiO_2, 34.8% Al_2O_3, and 13.8% MgO. Alumina, silica, and magnesia powders from (Iranian Nanomaterials Pioneers Company) with purity > 99% and particle size of 20µm were used as starting materials for cordierite ceramic. Table 1 shows the wet chemical analysis of each oxide.

Table 1: Wet Chemical Analysis of Silica, Alumina, and Magnesia

Alumina							
Oxide	**Al_2O_3**	**SiO_2**	**Fe_2O_3**	**MgO**	**CaO**	**Na_2O**	**K_2O**
%	99.80	0.03	0.002	0.04	0.06	0.25	0.008
Silica							
Oxide	**SiO_2**	**Al_2O_3**	**MgO**	**CaO**	**Fe_2O_3**	**Na_2O**	**K_2O**
%	99.80	0.07	0.02	0.04	0.03	0.02	0.02
Magnesia							
Oxide	**MgO**	**Al_2O_3**	**SiO_2**	**CaO**	**Fe_2O_3**	**Na_2O**	**K_2O**
%	**99.80**	**0.05**	**0.05**	**0.03**	**0.004**	0.006	0.25

To produce a homogenous mixture, the first starting oxides were wet mixed in a planetary ball mill at 400 rpm with ethanol alcohol as a dispersive medium for 4 hours. The resultant mixture was oven dried at 100°C for 24 hours before being finely crushed using a pestle and mortar. Particle size was determined using a laser particle size analyzer (Bettersize 2000), yielding a bimodal particle size of 2 µm as shown in Figure1.

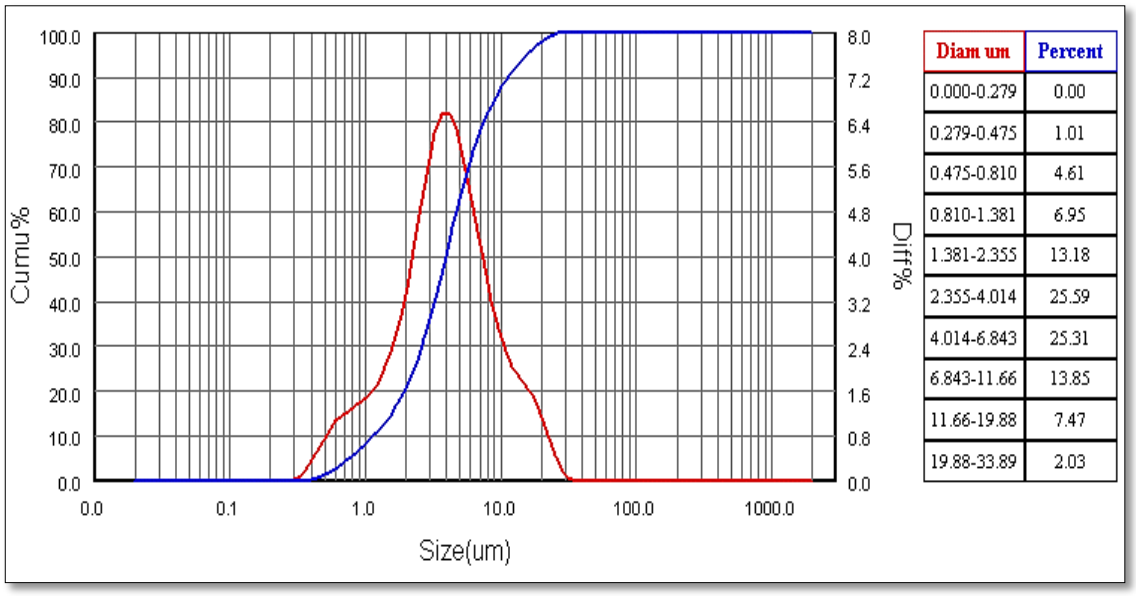

Figure 1: Particle Size Analysis of Mixed Oxides

Consequently, the powder blend was die pressed into a disc, cylindrical and rectangular samples under 5ton pressure, using polyvinyl alcohol (PVA) as binder material during pressing. Green specimens were dried at 100°C for 24 hours. The sintering stage was performed at 1400°C for two hours with 8°C/min as an average heating rate. As a final step, sintered cordierite samples were crushed into small pieces using a pestle and mortar and then ground into a fine powder using a ball mill for 10 hours to achieve cordierite nanopowder with a typical particle size of 96 nm as shown in Figure 2.

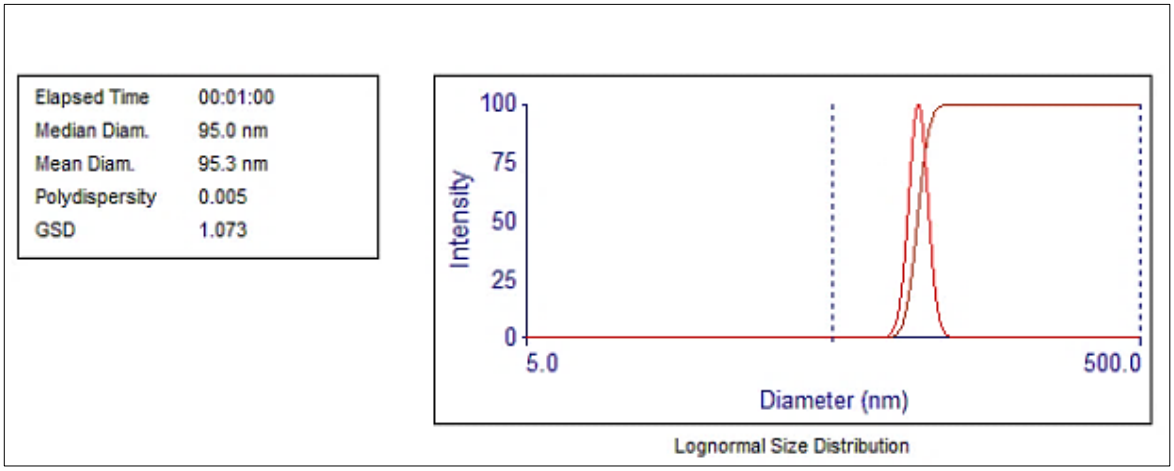

Figure 2: Particle Size Analysis of Prepared Cordierite Powder

2.2 Preparation of HA/Cordierite Powder

Hydroxyapatite nanopowder with needle-like particles (D = 10-30 nm, L=200nm, Pardis Technology Park, Tehran, Iran) was used in this study. During this stage, three batches of HA:Cordierite (70:30, 60:40, and 50:50) were prepared. Cordierite nanopowder by 30, 40, and 50 wt% was wetly mixed with hydroxyapatite nanopowder using a planetary ball mill in ethyl alcohol as dispersion media for 3 hours to obtain a homogeneous mixture. The resulting mixture was oven dried for 24 hours at 100 °C to burn out all dispersive media. Finally, the mixture isfinely milled using a pestle and mortar.

The powder mixture was die pressed into different specimen shapes via cold die pressing, using a hydraulic press machine at 5 tons using polyvinyl alcohol (PVA) as binder material. Green specimens dried out at 100°C for 24 hours to remove the organic binder phase. Dried specimens have been sintered at different temperatures 700, 900, and 1100°C for two hours with 10 °C/min as an average heating rate, Table 2 shows the composition of prepared samples.

Table 2: Composition of Cordierite/ Hydroxyapatite Bioceramic

NO.	Hydroxyapatite Wt%	Cordierite Wt%	Sintering Temperatures,°C
Z1	50	50	1100
Z2	50	50	900
Z3	50	50	700
Z4	60	40	1100
Z5	60	40	900
Z6	60	40	700
Z7	70	30	1100
Z8	70	30	900
Z9	70	30	700

3. Characterization

The phase was evaluated using x-ray diffractometry (Shimadzo, 6000) at room temperature with Cukα radiation (λ = 1.5405 Å), a scanning speed of 5°/min from 5° to 65° of 2θ (Bragg angle), and an applied power of 40 kV/30 mA. The size of crystals was determined using the Scherrer equation, as follows:

$$\beta cos\theta = \frac{0.9\,\lambda}{D} \quad (1)$$

Where Θ is the Bragg diffraction angle, D is the crystal size, λ is the radiation wavelength, is half of the diffraction peak width, and 0.9 is the Scherrer constant. The surface microstructure and the crystal size of the samples were investigated by Scanning Electron Microscope (SEM) instrument (Zeiss-Sigma-VP FE-SEM) to produce images with magnifications of (X15,000). The hardness of polished and sintered samples was determined using (Digital Microhardness Tester). All samples were polished using polishing papers and tested at 9.8 N with a time of 15 seconds withan average of five samples taken as representative values. The compressivestrength of all sintered samples having dimensions of 10 mm in diameter and 20 mm in height were tested using a microcomputer-controlled electronic universal testing machine (WDW-5E) with 50 KN load, a test speed of 0.5 mm/min and with an average of five samples for each value by employing the following relation:

$$\sigma = F/A \quad (2)$$

Young modulus was evaluated from the stress-strain curve generated during the compression test.

4. Results and Discussion

4.1 XRD Patterns

X-ray diffraction has been used in order to identify the resulting phases and evaluate the effect of sintering temperatures on the percent of each phase.

Figure 3.a depicts the XRD patterns of crystallization behavior of synthesized cordierite sintered at 1400 °C, its confirmed with the card code (01-084-1222). Also, Figure 3.b shows the XRD patterns of hydroxyapatite that are consistentwith the reference code (01-074-0566), which reveals that all diffraction peaks belong to the hydroxyapatite phase. Figure 4.a shows XRD patterns of Z3 sample that was prepared via sintering of (HA:Cordierite) with (50:50)wt.%.

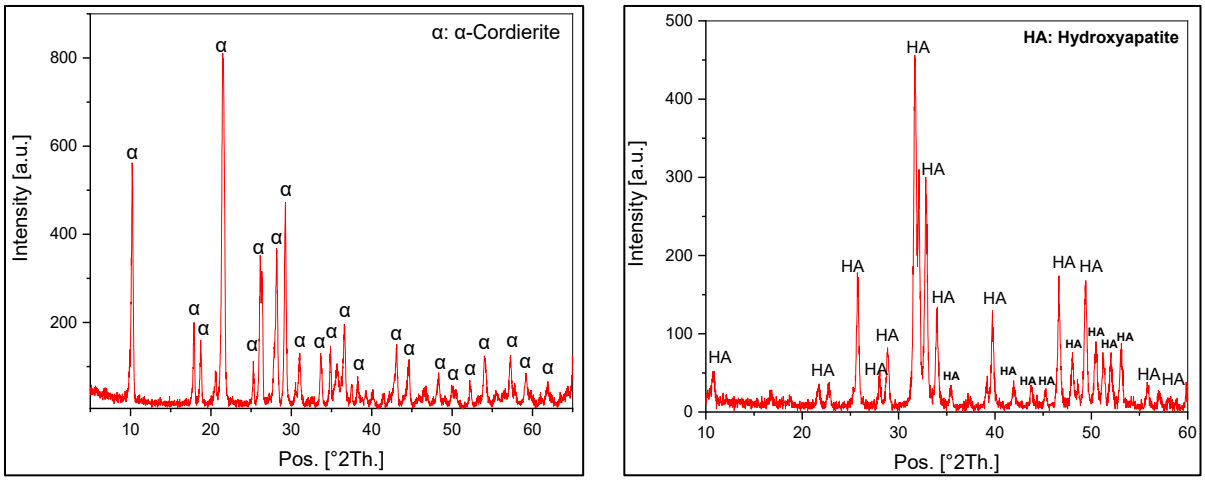

Figure 3: XRD Patterns of Cordierite (a) and HA (b)

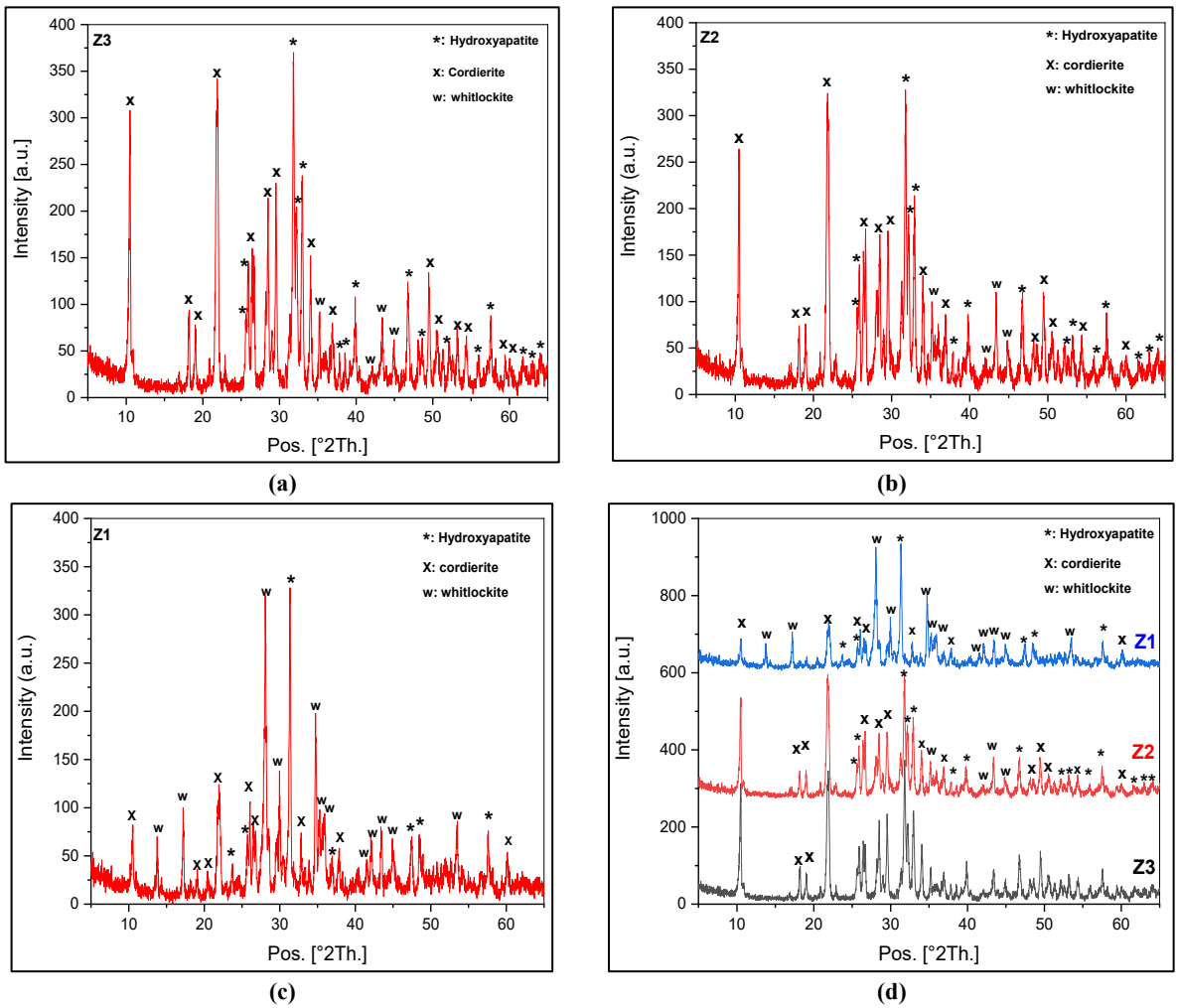

Figure 4: XRD patterns of Cordierite/HA samples prepared from 50wt% cordierite and 50wt% HA sintered at 700°C (a), 900°C (b), 1100°C (c) and crystallization behavior of the first batch (d)

In diffractogram of Z3, very small peaks at 2θ = 35.218, 42.064, 43.404, and 44.910 were consigned to the magnesium whitlockite phase (Calcium Magnesium Hydrogen Phosphate, $Ca_{18}Mg_2H_2$ $(PO_4)_{14}$) have been detected, which consistent with the reference code (00-042-0578). This indicates that a small amount of HA had reacted with magnesium that was released from cordierite crystals to form a whitlockite phase during the heating at 700°C. The main strong peaks of HA and cordierite have still stayed, this is because the temperature of 700°C is insufficient to cause the decomposition of cordierite – the highly chemically inert phase and hydroxyapatite. As the temperature increased to 900°C, many of the cordierite and HA strong peaks have been exhibited a reduction in their intensities, as observed in Figure 4.b. This behavior accompanied by increasing the

intensity of previously available whitlockite peaks as the temperature raised to 900°C in sample Z2, while magnesium whitlockite peaks at 2θ = 42.11, 43.404 and 44.879 exhibit an increase in their intensity and sharpness. During the sintering of the mixture at 1100 °C, new whitlockite peaks had been appearing at 2θ = 13.769, 17.192, and 41.566. The main strong peaks of cordierite at 2θ = 10.524 and 21.965 became very small and weak peaks. Furthermore, secondary cordierite peaks have been highly decreased. The main hydroxyapatite peak appears at 2θ = 31.346 in Figure 4.c had been shifted and reacted with cordierite to form magnesium whitlockite ($Ca_{18}Mg_2H_2$ $(PO_4)_{14}$), which became the prominent phase at the sintering temperature of 1100°C [17]. Also, the peak that appears at 2θ = 34.897 became more intense and sharper which belongs to magnesium whitlockite. All of the magnesium whitlockite peaks which appeared previously at 700 and 900°C increased in intensity and sharpness.

All HA peaks at positions ranging from 60° to 65° completely disappear. The behavior of the sample prepared from 50:50 HA:Cordierite is represented in Figure 4.c. Figure 4.d shows the crystallization behavior of Batch 1. The samples of the second batch have exhibited the same behavior as the previous samples of the first batch. The percent of the magnesium whitlockite phase is much less than that formed in the first batch. This is due to the second mixture including 40 wt.% of cordierite phase, i.e. lower magnesium content that would have reacted with HA to form magnesium whitlockite phase. The number and intensity of this phase peaks increased gradually with increasing sintering temperatures,Figure 5.a shows this behavior. When the temperature raised to 900°C, all Mg-whitlockite peaks, that formed previously, have been increased in their intensity without the formation of any new Mg-whitlockite peaks at this temperature, Figure 5.b revealed XRD patterns of sample Z5.

Figure 5.c shows the heat treatment behavior at 1100°C, new Mg-whitlockite peaks have appeared at 13.469, 17.781, 26.750, 27.786, 34.728, 41.463, 44.986, 48.613, and 59.803. In addition to this formation, the previous peaks have been becoming strong in their intensity.Figure 5.d above illustrates the XRD patterns of HA/Cordierite by (60:40) wt.% and sintered at 700, 900, and 1100 °C, they are denoted Z6, Z5, and Z4 respectively.

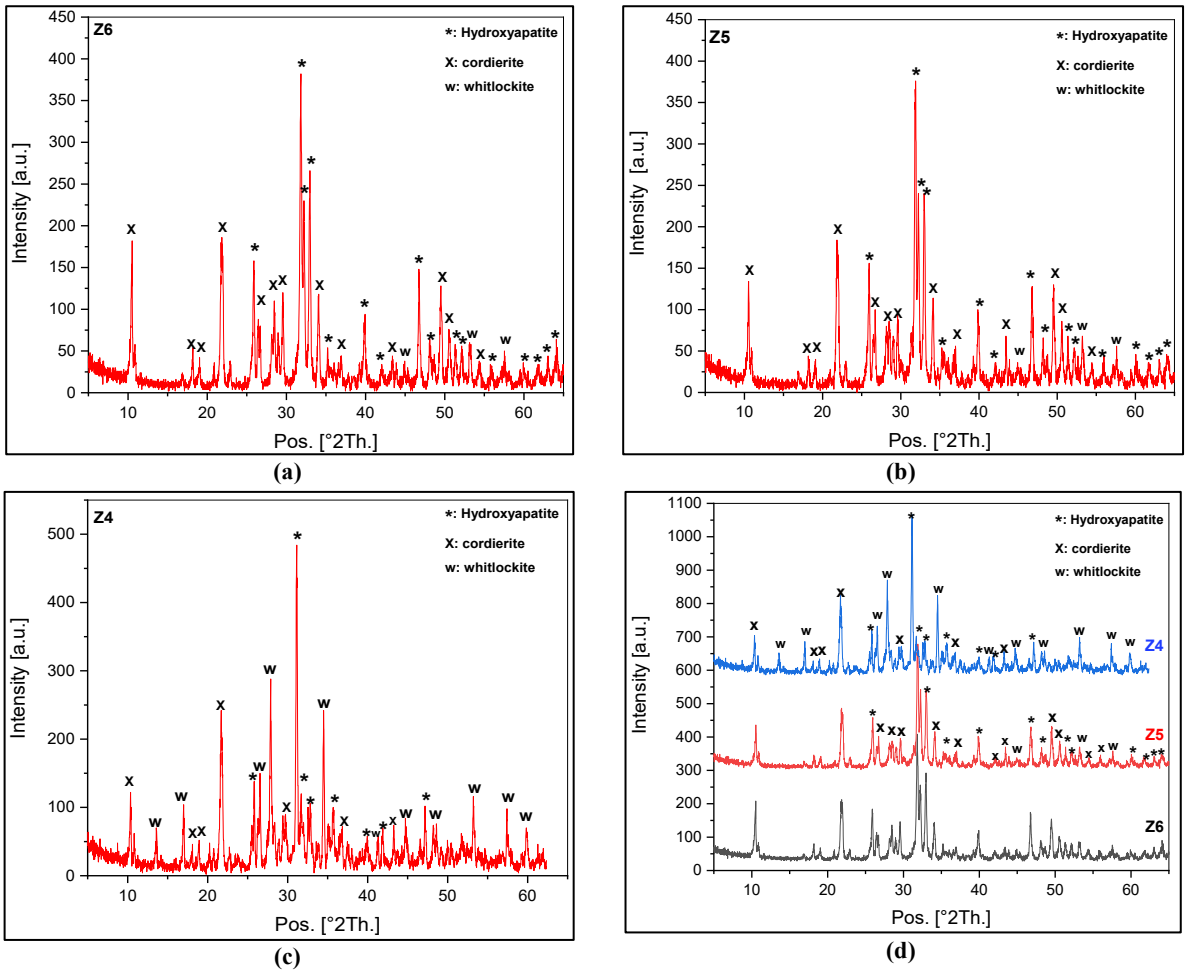

Figure 5: XRD patterns of HA/Cordierite samples prepared from 40 wt% cordierite and 60 wt% HA sintered at 700°C (a), 900°C (b), and 1100°C (c) and crystallization behavior of the second batch (d)

The third batch involves samples prepared by sintering of Cordierite:HA = 30:70, sintered at 700, 900, and 1100 °C denoted as Z9, Z8, and Z9 respectively. In Figure 6.a which revealed XRD patterns of Z9, the most predominated phase was hydroxyapatite. A very little part of HA reacted with cordierite and resulted in Mg-whitlockite phase creation due to heat treatment at 700°C.The intensity of these peaks increased gradually as the sintering temperature raised from 700 to 1100 °C.When the temperature upraised to 900°C, all Mg-whitlockite peaks, that formed previously, have increased in their intensity with the formation of a new Mg-whitlockite peak at this temperature, Figure 6.b shows this behavior.

During the heat treatment at 1100 °C, new Mg-whitlockite peaks appeared at 2θ°= 13.469, 17.781, 20.381, and 33.929 as proposed in Figure 6.c. Figure 6.d shows XRD patterns of samples Z9, Z8, and Z7 heat treated at 700, 900, and 1100°C respectively. This batch of samples behaves the same as the previous bathes. The presence of Mg-whitlockite matched with the literature [18,19] and standard code (01-070-2064).

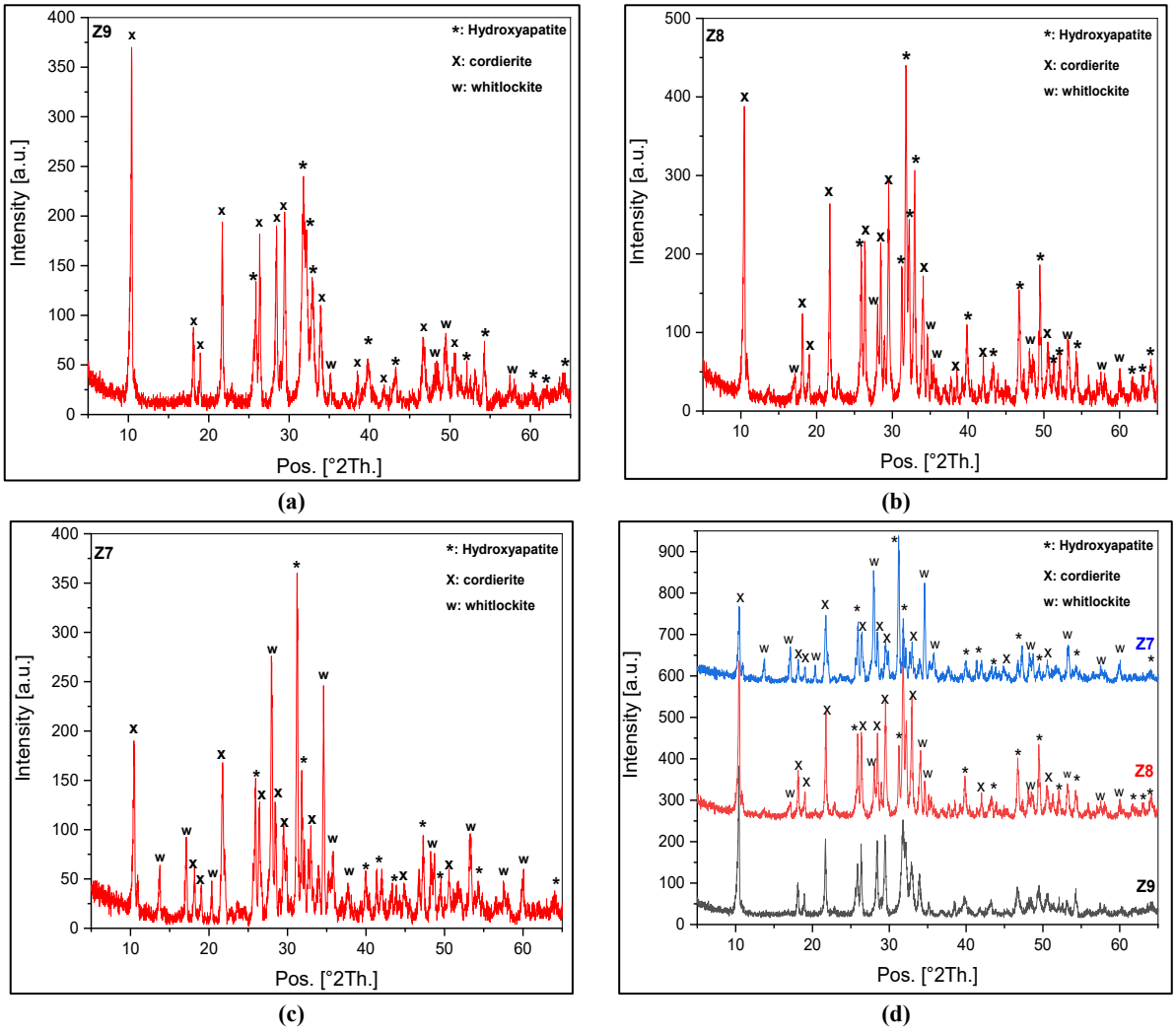

Figure 6: XRD patterns of Cordierite/HA samples prepared from 30wt% cordierite and 70wt% HA sintered at 700°C (a), 900°C (b), and 1100°C (c) and crystallization behavior of the third batch (d)

4.2 Scanning Electron Microscope (SEM)

Microstructures of all prepared samples have been characterized using SEM. The SEM images of samples prepared from 50:50 (HA:cordierite) and sintered at 700, 900, and 1100°C are shown in Figure 7.a,b, and c respectively. As it is seen in image a, there is a homogeneous very fine grain with good acceptable densification. In addition, there is an appearance of interconnected and closed pores, which had been referred to by the red and green arrows respectively; these are a consequence of the evaporation of binder material. As the treatment temperature was raised to 900°C, the microstructure of Z2 sample, depicted in image b, became more uniform in terms of grain size distribution and grain coalescence. This was companied by considerable crystallite growth and densification as compared with the previous sample. The morphology of Z1 sample treated at 1100 °C is represented in image c. The image shows that there is a very clear development in the particle size accompanied by the appearance of grains coalescence that resulted in a higher densification. Figures 8.a,b, and c depicted the morphology of the batch comprising 40:60 (Cordierite:HA) sintered at 700, 900, and 1100°C respectively. Image a, illustrates the morphology of sample Z6, whichdisplays extra fine crystallites, highly homogeneous and dense texture, and very limited numbers of micro-pores (marked with red arrows). As the temperature upraised to 900°C, an explicit granular growth appears within the microstructure of Z5 sample marked by the letter b and this was confirmed by examining the size of the crystals, which reveals the growth of crystallites, which increases with the increasing of sintering temperatures. The same behavior appears for the sample that was sintered at a temperature of 1100°C, bears the symbol Z4, and is marked by image c. Samples of the third batch prepared from 30:70 (Cordierite:HA) and sintered at 700, 900, and 1100°C have been obtained in Figure 9.a,b,c respectively. All samples exhibit the same behavior as in previous batches. There was a clear grain growth, which increased dramatically in samples sintered at 1100°C companied by the formation of cracks, marked by the red arrow. This grain growth is attributed to the absorption of heat energy by the particles[20]. A large number of tiny, small particles are linked, resulting in

irregular agglomerated clusters [7]. The major crucial aspect for improving the mechanical characteristics of ceramic materials is a fine and homogenous microstructure [21,22].

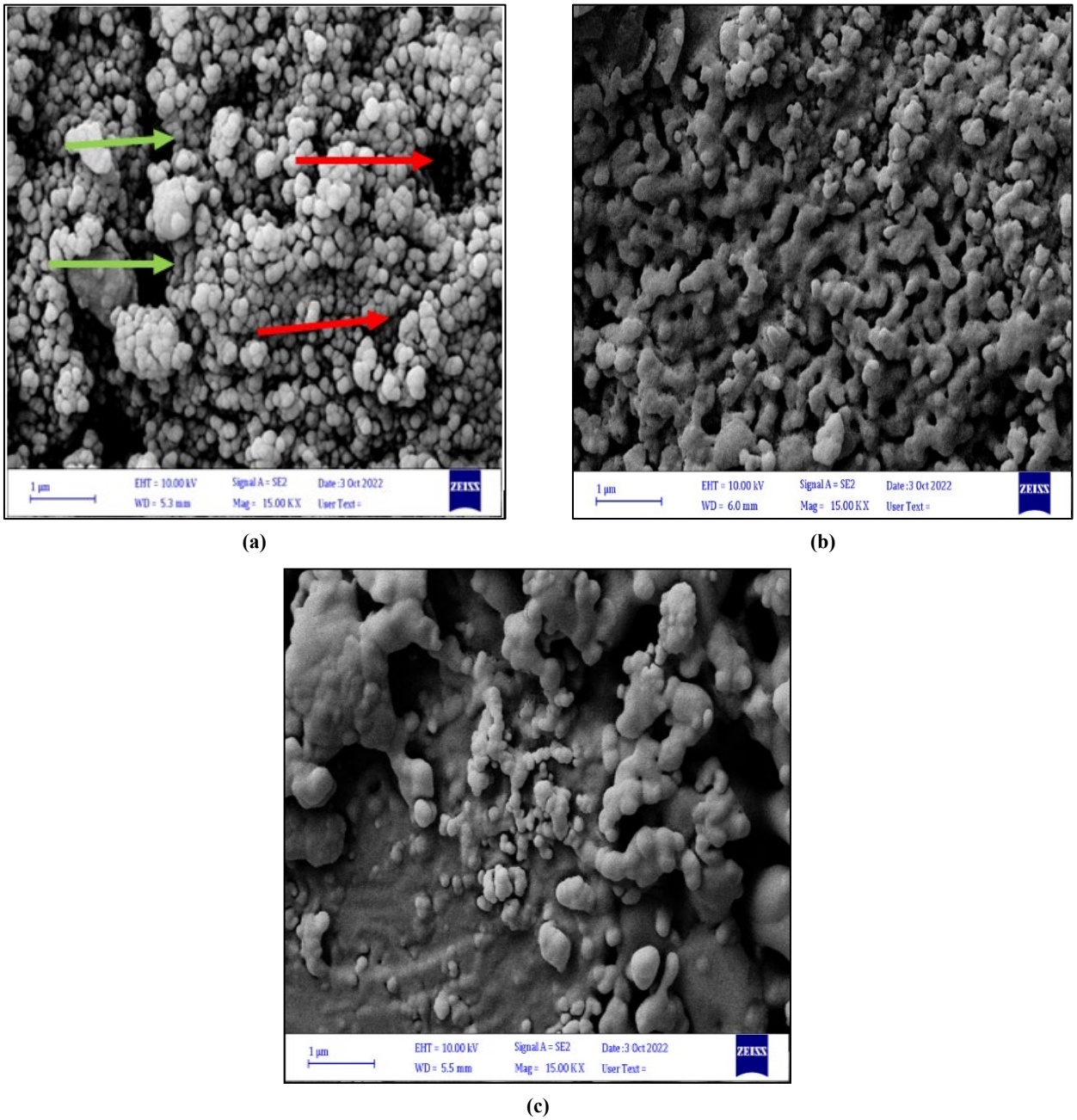

(a) **(b)**

(c)

Figure 7: SEM Micrograph for Z3 (a), Z2 (b), and Z1(c)

4.3 Crystallite Size

Mean crystallite sizes grown at different temperatures calculated using Scherrer equation are listed in Table 3.

Table 3: Crystallite Size of Cordierite / Hydroxyapatite Samples

Sample	Crystallite Size (nm)		
	700 °C	**900 °C**	**1100 °C**
Cor		60.025	
HA	30.01	32.22	35.71
Batch 1	36.29	39.54	40.30
Batch 2	33.94	38.88	39.46
Batch 3	34.97	39.36	39.84

Figure 10 depicts crystallite size as a function of sintering temperature for the three batches. However, the crystallite sizes, calculated according to XRD patterns with full-width maximum half, increased gradually with increasing sintering

temperatures, when the size of 36.295 nm at 700°C slightly increased to 39.544 nm at 900 °C, and finally to 40.3 nm at 1100°C in the first batch. This behavioris attributed to the fact of increasing treatment temperatures causes grain growth and agglomeration of fine particles as a result of diminishing the internal energy of the system [16]. The geometry of all particles was sphere-like as represented by SEM imaging. This is a very important requirement for the application of Debye-Sherrer equation to estimate the crystallite size. This equation should be applied to determine crystallite sizes of samples with sphere-like geometry because the constant 0.89 applies only to spherical shapes[19].

On the other hand, the term crystallite sizes are not suitable for needle-like or rod-like particles or any other type of geometries, because such types of shapes require more than two parameters to determine their sizes [23]. Therefore, there is a good correlation between crystallite size determinations and SEM images.

The crystallite size of all samples exhibited the same behavior with increasing sintering temperatures. These results are in high accordance with those reported by Sadeghzade et. al [20]. Grain growth is a phenomenon that occurs after recrystallization when the strain-free grains continue to grow if the specimen is left at elevated temperatures. Reduction of high energy is the driving force for grain growth. It represents an increase in average grain size in polycrystalline materials [24,25]. At constant temperature, increasing the crystallite sizes with increasing the cordierite percent from 40 to 50 wt.% is attributed to decreasing the lattice strain and grain boundaries. This is consistent with SEM imaging which also can be justified by decreasing dislocation density with an increase in cordierite content [26].

As compared with the crystallite size of control samples, that comprising HA only, the addition of cordierite result in slight grain growth, i.e. cordierite cause little increase in crystallite size.

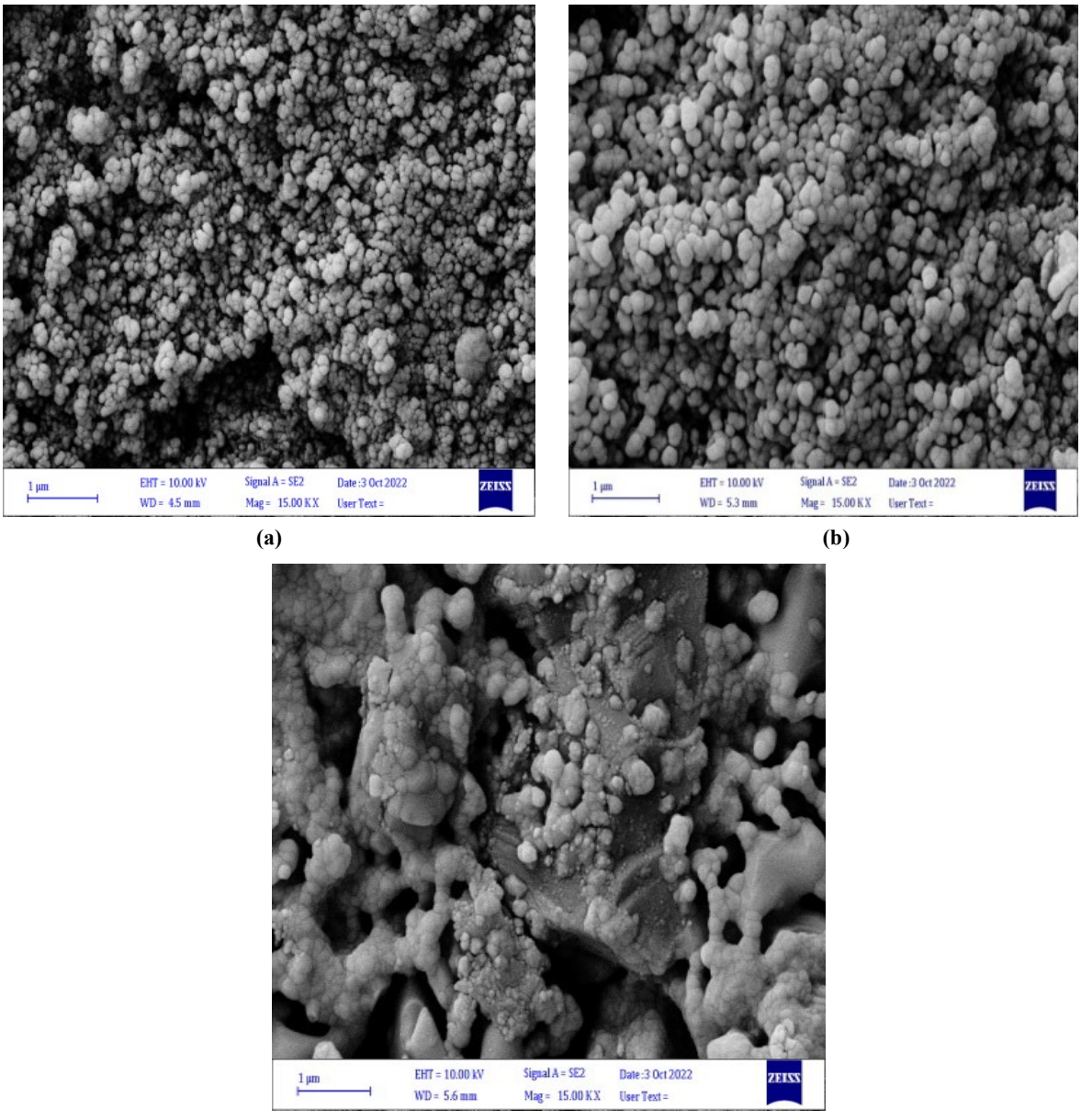

Figure 8: SEM Micrograph for Z6 (a), Z5 (b), and Z4(c)

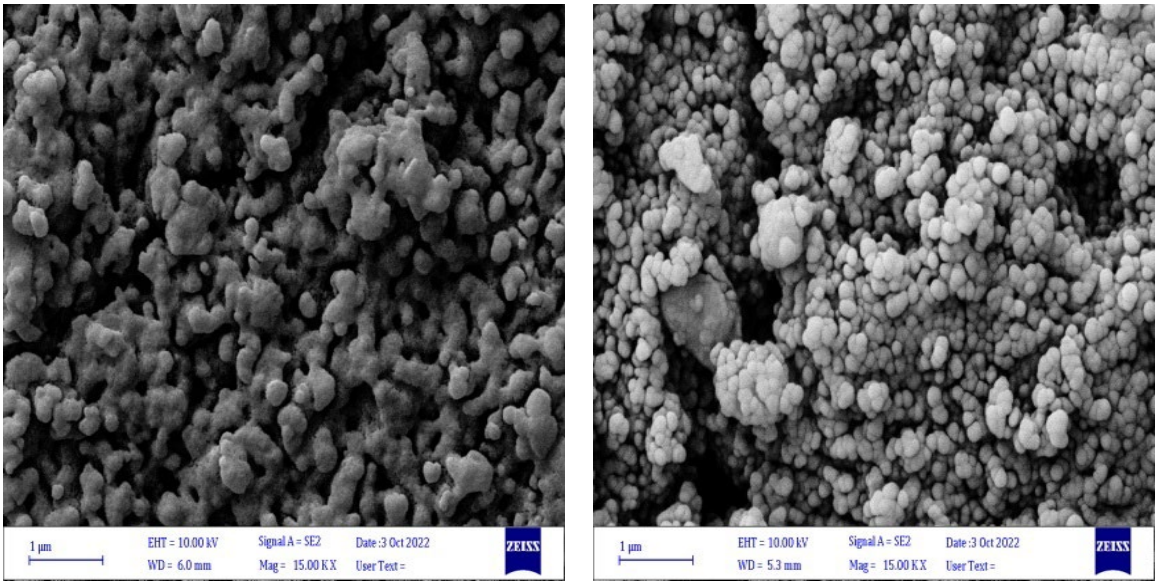

(a) **(b)**

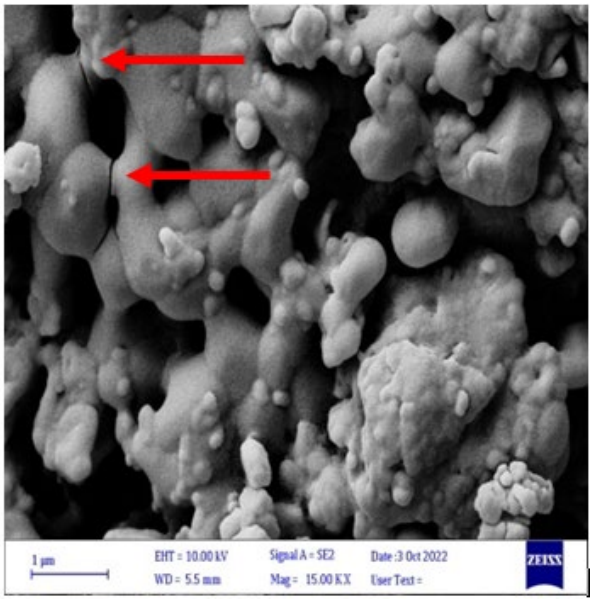

(c)

Figure 9: SEM Micrograph for Z9 (a), Z8 (b), and Z7(c)

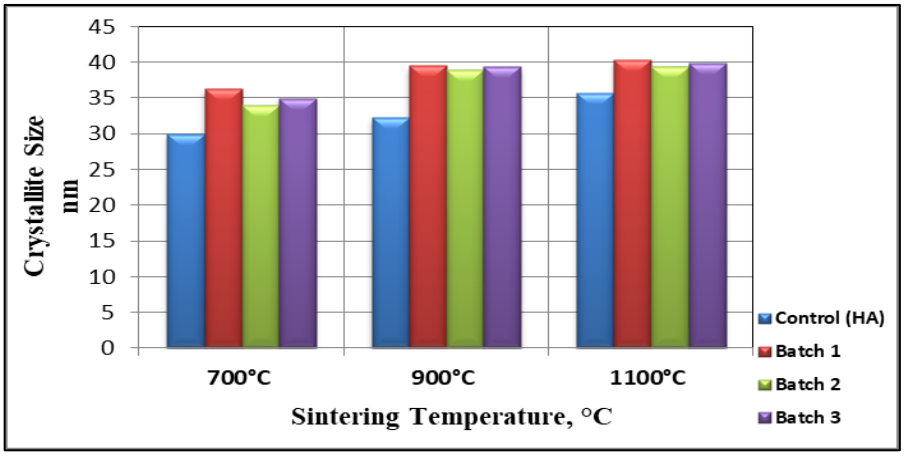

Figure 10: Crystallite Size Versus the Sintering Temperatures of Prepared Batches

4.4 Vickers' Micro-hardness

The micro-hardness test is the most accurate. This test is very suitable for testing polished and hardened materials due to the small impression made on testing specimens. Its' values are represented as (Hv) and in order to convert micro-hardness values from Hv to GPa, its multiplied by (0.009807). Figure 11 and Table 4 show hardness in GPa as a function of sintering temperature for all batches. In the first batch, that comprising 50 wt.% cordierite and 50 wt.% hydroxyapatite, it has been observed that there is a relative increase in hardness values with increasing sintering temperature.

It has been found that the hardness of sample (Z3), which was sintered at 700°C is 5.62 GPa. This value increased to 6.47 GPa as the sintering temperature upraised to 900 °C and eventually became 7.03 GPa during the heat treatment at 1100°C. This phenomenon is attributed to the degree to which the microstructure improved as sintering temperatures increased. At the greatest sintering temperature of 1100°C, denser and more uniform pore geometry with more round pore geometry was found (as illustrated by SEM images), and the values (7.03 GPa), are higher than that of human femoral cortical bone.

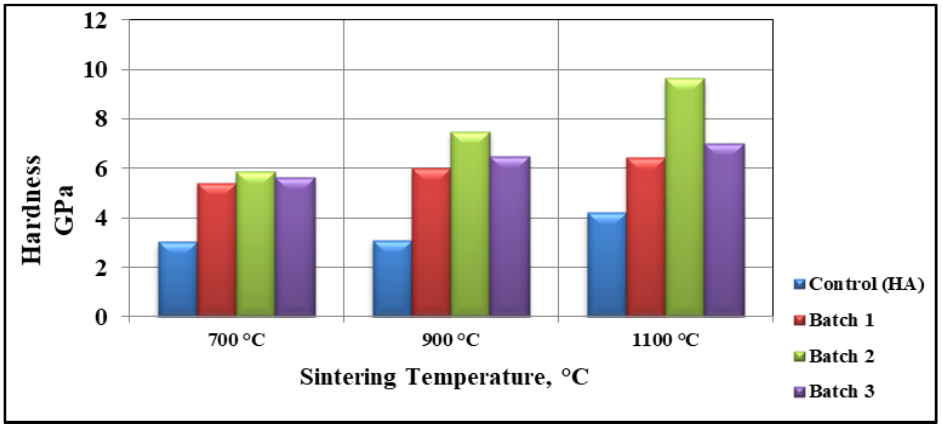

Figure 11: Hardness Versus the Sintering Temperatures of Prepared Batches

In the second batch, the hardness of 5.86 GPa at 700°C, increased suddenly to 7.48 GPa at 900°C and then to 9.64 at 1100 °C. Samples of batch 2 demonstrate the greatest values for hardness. This is attributed to their unique microstructure and very fine crystallite sizes, that are consistent with SEM and mechanical properties analysis. It can be concluded from the figure, that the first batch comprising 50 wt.% of cordierite, shows the lowest hardness value. This behavior is consistent with XRD analysis, which demonstrates that as the cordierite percent increases, the percent of Mg-whitlockite phase increases. Consequently, there is a slight reduction in hardness values, because whitlockite is an atri-calcium phosphate phase that has mechanical properties smaller than these of hydroxyapatite. At the highest sintering temperature (1100°C), SEM pictures revealed a more dense structure and great homogeneity in pore morphologies with additional round pore geometry; the values of all samples are higher than those of human femoral cortical bone.

As cordierite percent increase from 30% to 40%, there is a clear increase in the values of hardness. This is attributed to decreasing the grain sizes of the second batch, and the behavior follows the Hall-Petch (H-P) relationship, which proposed that the mechanical properties increase with decreasing the grain size [27]. Hardness increased for the second batch as compared with the other two batches, because it had the finest microstructure. Consequently, decreasing the grain size resulted in reducing the free path for dislocation motion, and thus, stronger material was resulted [27,28]. Usually, the cortical bone is 10-15% harder than the cancellous bone adjacent in orientation. Therefore, experimentally, all samples are suitable for load-bearing bones.

4.5 Compressive Strength

Figure12 shows the compressive strength as a function of sintering temperatures. It has been predicted that the compression strength slightly increases with increasing of sintering temperatures. The strength value was 36.40 MPa at a temperature of 700 °C, increased slightly to become 39.78 MPa at 900 °C, and eventually has been settled at 41.47 MPa when the temperature was 1100 °C. This behavior may be attributed to increasing the perfection of microstructure with increasing sintering temperature and this is consistent with SEM imaging [15]. Also, the grain growth (increasing of crystallite size), that occurs with upraising the heat treatment temperatures, was inconsiderably slight, i.e. from 36.3 to 40.3 nm. This means the crystallite growth was only 11%, and such a low percentage does not greatly affect the mechanical performance of samples that belong to the same batch.

It can be noted from Figure 12, that for batch 2, the compressive strength of 38.76 MPa at 700°C and 41.23 MPa at 900°C, and these values increased gradually to reach 50.41 MPa at 1100°C. The samples of the other third batches exhibit the same behavior with the treatments' heat. This performance can be justified by the perfection of the samples' microstructure, i.e. absence of impurities, porosity, cracks, and any other types of lattice imperfections [15]. Mechanical strength data show great consistency with SEM pictures, which show superb grain coalescence and a dense structure with no holes, indicating the occurrence of a suitable reaction between reacting components.

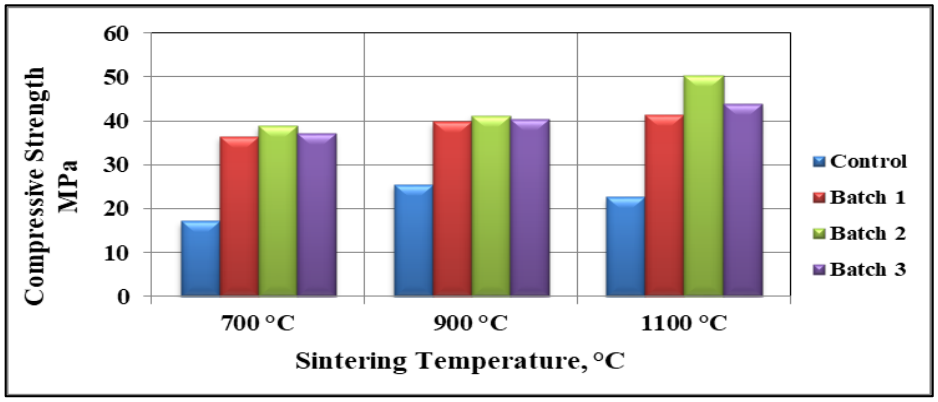

Figure 12: Compression Strength Versus the Sintering Temperatures of Prepared Batches

At constant temperature, it has been noted, that increasing cordierite percent from 30 to 40 wt.% resulted in improved strength, while batch 1, which comprises 50 wt.% cordierite and 50 wt.% HA exhibits values lower than that of the other two percent. The second batch employs the highest values as compared with others. These results are consistent with crystallite sizes. In other words, increasing cordierite content from 30 to 40 wt.% results in decreasing crystallite sizes, i.e. finer microstructure, which in turn employed higher compressive strength. This behavior can be justified according to Hall-Petch (H-P) relationship [29,30].

Decreasing the grain size is regarded as one of the strengthening mechanisms in materials, which knowing as strengthening by grain size reduction [25]. The smaller the grain size, the higher the number of grains available, which means the larger the number of grain boundaries that will act as an obstacle to dislocation motion. The obstruction or hindrance of dislocation motion in materials is the foundation of materials' strengthening [25]. As cordierite percent increased from 40 to 50 wt.%, the crystallite sizes increased in all samples of batch 1, and for this reason, the compressive strength of batch 1 samples' were slightly less than those of batch 2 samples. This is attributed to the fact, that increasing grain size resulted in higher free paths for dislocation motion, and consequently decreasing in mechanical performance [27,30].

4.6 Modulus of Elasticity (E)

In this study, the modulus of elasticity had been determined from the stress-strain curve during compression testing. The results of the test are observed in Table 4, where the property of each sample is recorded as a function of sintering temperatures and cordierite percent. Figure 13 shows this relationship. Almost, the behavior of E is similar to that of hardness and compressive strength. In each batch, E increase with increasing sintering temperature. This is consistent with the SEM result, which illustrated highly homogeneous microstructure and increasing densification with the temperature upraising.

The second batch, that contains 60% HA and 40% wt. cordierite, employing the highest values for modulus of elasticity at all temperatures. This is attributed to the perfection of the microstructure of batch two samples', which exhibits a finer grain size as compared with other batches. Consequently, and according to Hell-Petch law, the mechanical properties increase with decreasing grain size. From Table 4 and Figure 13, the values of E range between 15-37 GPa, which highly consistent with that of cortical bone [31].

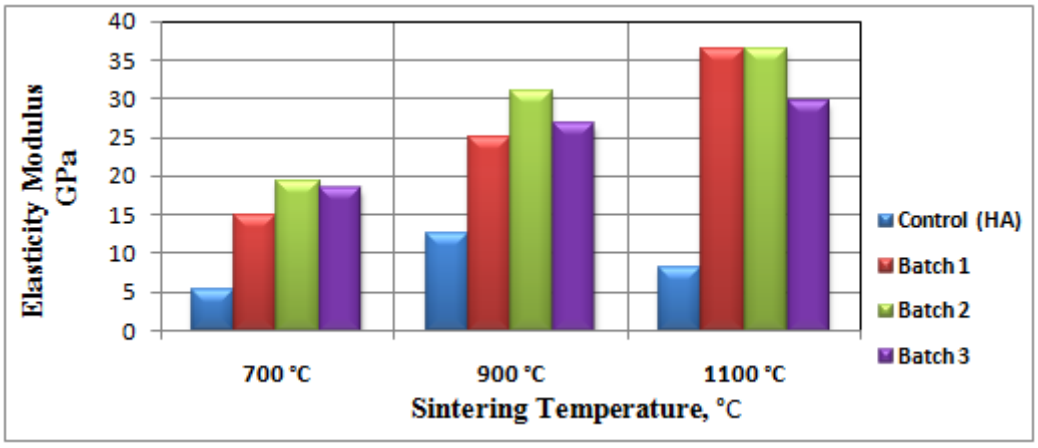

Figure 13: Elastic Modulus Versus the Sintering Temperatures of Prepared Batches

Table 4: Mechanical Properties of Hydroxyapatite/Cordierite Samples

Sample	Hardness (GPa)			Compressive Strength (MPa)			Young Modulus (GPa)		
	700 °C	900 °C	1100 °C	700 °C	900 °C	1100 °C	700 °C	900 °C	1100 °C
Cor		12.87			166.45			145	
HA	3.02	3.61	4.22	17.13	25.52	22.66	5.22	12.45	8.09
Batch 1	5.42	6.01	6.45	36.40	39.78	41.47	15.00	25.03	36.30
Batch 2	5.86	7.48	9.64	38.76	41.23	50.41	19.35	31.00	36.50
Batch 3	5.62	6.47	7.03	37.04	40.27	43.92	18.42	26.68	29.56

5. Conclusion

Cordierite is magnesium aluminum silicate, that had been successfully incorporated with hydroxyapatite and resulted in a novel biomaterial with improved properties as cordierite a biocompatible ceramic with high mechanical characteristics. Results show that all of the samples, which contain different percents of nano cordierite powder, at all temperatures have significant mechanical properties as compared with the control sample (without cordierite additions). The incorporation of cordierite caused a slight increase in grain size at all sintering temperatures. A 30% cordierite increased the compressive strength of HAby 116.23% at 700 °C, 57.80% at 900 °C, and 94.34 % at 1100 °C. While, the effect of this cordierite on hardness, was increasing by 86.09% at 700 °C, 108.71% at 900 °C, and 66.59 % at 1100 °C.

A 40% cordierite increased the compressive strength of HA by 126.27 % at 700 °C, 61.52 % at 900 °C, and 123.05 % at 1100 °C. While, the effect of this cordierite level on hardness, was increasing by 94.04% at 700°C, 141.29 % at 900°C, and 128.44 % at 1100 °C. A 50% cordierite increased the compressive strength of HA by 112.37 % at 700°C, 55.88 % at 900°C, and 83.50 % at 1100 °C. While, the effect of this cordierite content on hardness was increasing by 79.47% at 700 °C, 93.87 % at 900 °C, and 52.84 % at 1100 °C. Modulus of elasticity exhibit behavior as that of compressive strength and hardness. Its value shows excellent consistency with these cortical bones. Among all ratios, the second mixture, which includes 40% cordierite and 60% HA, is the one that shows the best mechanical properties at all sintering temperatures.

Author contribution

All authors contributed equally to this work.

Funding

This research received no specific grant from any funding agency in the public, commercial, or not-for-profit sectors.

Data availability statement

Not applicable.

Conflicts of interest

The authors of the current work do not have a conflict of interest.

References

[1] T. Zhang, W. Cai, F. Chu, F. Zhou, S. Liang, C. Ma, Y. Hu, Hydroxyapatite/polyurea nanocomposite: Preparation and multiple performance enhancements, Compos. Part A Appl. Sci. Manuf., 128 (2020) 105681.https://doi.org/10.1016/j.compositesa.2019.105681

[2] C. Ruiz-Aguilar, U. Olivares-Pinto, I. Alfonso, Novel β-TCP scaffold production using NaCl as a porogen for bone tissue applications, Ceram. Int., 47 (2020) 2244-2254.https://doi.org/10.1016/j.ceramint.2020.09.064

[3] M. J. Hossan, M. A. Gafur, M. M. Karim, A. A. Rana, Mechanical properties of Gelatin Hydroxyapatite composite for bone tissue engineering, Bangladesh J. Sci. Ind. Res., 50 (2015) 15-20.https://doi.org/10.3329/bjsir.v50i1.23805

[4] M. Safarabadi, N. Khansari, A. Rezaei, An experimental investigation of HA/Al_2O_3 nanoparticles on mechanical properties of restoration materials, Eng. Solid Mech., 2 (2014)173-182.

[5] D. J. Curran, T. J. Fleming, M. R. Towler, S. Hampshire, Mechanical properties of hydroxyapatite–zirconia compacts sintered by two different sintering methods, J. Mater. Sci. Mater. Med., 21 (2010) 1109-1120.https://doi.org/10.1007/s10856-009-3974-z

[6] S. Baradaran, E. Moghaddam, W. J. Basirun, M. Mehrali, M. Sookhakian, M. Hamdi, Y. Alias, Mechanical properties and biomedical applications of a nanotube hydroxyapatite-reduced graphene oxide composite, Carbon, 69 (2014) 32-45.https://doi.org/10.1016/j.carbon.2013.11.054

[7] M. Taherian, R. Rojaee, M. Fathi, M. Tamizifar, Effect of different sol-gel synthesis processes on microstructural and morphological characteristics of hydroxyapatite-bioactive glass composite nanopowders, J. Adv. Ceram., 3 (2014) 207-214. https://doi.org/10.1007/s40145-014-0111-3

[8] X. Chen, B. Zhang, Y. Gong, P. Zhou, H. Li, Mechanical properties of nanodiamond-reinforced hydroxyapatite composite coatings deposited by suspension plasma spraying, Appl. Surf. Sci., 439 (2018) 60-65.https://doi.org/10.1016/j.apsusc.2018.01.014

[9] S. Chen, Y. Shi, X. Zhang, J. Ma, 3D printed hydroxyapatite composite scaffolds with enhanced mechanical properties, Ceram. Int., 45 (2019) 10991-10996.https://doi.org/10.1016/j.ceramint.2019.02.182

[10] Y. P. Guo, J.J. Guan, J. Yang, Y. Wang, C. Q. Zhang, Q. F. Ke, Hybrid nanostructured hydroxyapatite–chitosan composite scaffold: Bioinspired fabrication, mechanical properties, and biological properties, J. Mater. Chem. B, 3 (2015) 4679-4689.https://doi.org/10.1039/C5TB00175G

[11] Z. Wu, Z. Meng, Q. Wu, D. Zeng, Z. Guo, J. Yao, Y. Zhao, Biomimetic and osteogenic 3D silk fibroin composite scaffolds with nano MgO and mineralized hydroxyapatite for bone regeneration, J. Tissue Eng., 11 (2020) 1-21.https://doi.org/10.1177/2041731420967791

[12] M. Barabashko, A. Ponomarev, A. Rezvanova, V. Kuznetsov, S. Moseenkov, Young's Modulus and Vickers Hardness of the Hydroxyapatite Bioceramics with a Small Amount of the Multi-Walled Carbon Nanotubes, Materials, 15 (2022) 5304.https://doi.org/10.3390/ma15155304

[13] M .Nadafan, R.Malekfar, Z.Dehghani,Structural and optical properties of cordierite glass-ceramic doped in polyurethane matrix, AIP Advances, 5 (2015) 067135.https://doi.org/10.1063/1.4922838

[14] H.Ismail, H.Mohamad, Preliminary Study on the Bioactivity Properties of Cordierite/B-Wollastonite Biocomposite Ceramics,Key Eng. Mater., 908 (2022) 148-153.https://doi.org/10.4028/p-o96487

[15] M. M. Shukur, M. A. Asward, Z. J. Khadhim, Preparation of Cordierite Ceramic from Iraqi Raw Materials, Int. J. Eng. Technol., 5 (2015) 172-175

[16] C. Ghitulica, E. Andronescu, O. Nicola, A. Dicea, M. Birsan, Preparation and characterization of cordierite powders, J. Eur. Ceram. Soc., 27 (2007) 711-713.https://doi.org/10.1016/j.jeurceramsoc.2006.04.089

[17] R. Nawang, M. Z. Hussein, K. A. Matori, C. A. Abdullah, M. Hashim, Physicochemical properties of hydroxyapatite/montmorillonite nanocomposite prepared by powder sintering, Results Phys., 15 (2019) 102540.https://doi.org/10.1016/j.rinp.2019.102540

[18] H. L. Jang, K. Jin, J. Lee, Y. Kim, S. H. Nahm, K. S. Hong, K. T. Nam, Revisiting whitlockite, the second most abundant biomineral in bone: nanocrystal synthesis in physiologically relevant conditions and biocompatibility evaluation, ACS nano, 8 (2014) 634-641.https://doi.org/10.1021/nn405246h

[19] A. C. Tas, Transformation of Brushite (CaHPO4· 2H2O) to Whitlockite (Ca9Mg (HPO4)(PO4) 6) or other CaPs in physiologically relevant solutions, J. Am. Ceram. Soc., 99 (2016) 1200-1206.https://doi.org/10.1111/jace.14069

[20] S. Sadeghzade, R. Emadi, F. Tavangarian, M. Naderi, Fabrication and evaluation of silica-based ceramic scaffolds for hard tissue engineering applications, Mater. Sci. Eng. C, 71 (2017) 431-438.https://doi.org/10.1016/j.msec.2016.10.042

[21] B. Nasiri-Tabrizi, A. Fahami, R. Ebrahimi-Kahrizsangi, A. Khazraei, M. R. Yazdani, M. J. Kajbafzadeh, A study on mechanochemical behavior of CaO-P_2O_5-CaF_2–ZrO_2 system to produce fluorapatite–zirconia composite nanopowders, Powder Technol., 243 (2013) 59-70.https://doi.org/10.1016/j.powtec.2013.03.034

[22] M. Esnaashary, M. Fathi, M. Ahmadian, The Effect of the Two-Step Sintering Process on Consolidation of Fluoridated Hydroxyapatite and its Mechanical Properties and Bioactivity, Int. J. Appl. Ceram. Technol., 11 (2014) 47-56.https://doi.org/10.1111/ijac.12053

[23] W. P. S. L. Wijesinghe, M. M. M. G. P. G. Mantilaka, E. V. A. Premalal, H. M. T. U. Herath, S. Mahalingam, M. Edirisinghe, R. M. G. Rajapakse, Facile synthesis of both needle-like and spherical hydroxyapatite nanoparticles: Effect of synthetic temperature and calcination on morphology, crystallite size and crystallinity, Mater. Sci. Eng. C, 42 (2014) 83-90.https://doi.org/10.1016/j.msec.2014.05.032

[24] W. Khoo, F. M. Nor, H. Ardhyananta, D. Kurniawan, Preparation of natural hydroxyapatite from bovine femur bones using calcination at various temperatures, Procedia Manuf., 2 (2015) 196-201.https://doi.org/10.1016/j.promfg.2015.07.034

[25] Callister,W. D. andRethwisch, D. G. Materials science and engineering: an introduction, New York: John wiley& sons, 2007.

[26] K. Venkateswarlu, M. Sandhyarani, T. A. Nellaippan, N. Rameshbabu, Estimation of crystallite size, lattice strain and dislocation density of nanocrystalline carbonate substituted hydroxyapatite by X-ray peak variance analysis, Procedia Mater. Sci. , 5 (2014) 212-221.https://doi.org/10.1016/j.mspro.2014.07.260

[27] J. Wang, L.L. Shaw, Nanocrystalline hydroxyapatite with simultaneous enhancements in hardness and toughness, Biomaterials, 30 (2009) 6565-6572.https://doi.org/10.1016/j.biomaterials.2009.08.048

[28] Z. Ali, F. Al-Hasani, Investigating the Effects of Nano Ceramics based Pack Cementation Coatings on Properties of some Biomedical Ti Alloys, IOP Conf. Ser. Mater. Sci. Eng., 1094 (2021) 012167. https://doi.org/10.1088/1757-899X/1094/1/012167

[29] Z. Shen, M. Johnsson, Z. Zhao, M. Nygren, Spark plasma sintering of alumina, J. Am. Ceram. Soc., 85 (2002)1921-1927.https://doi.org/10.1111/j.1151-2916.2002.tb00381.x

[30] A. Bellosi, D. Sciti, S. Guicciardi, Synergy and competition in nano-and micro-design of structural ceramics, J. Eur. Ceram. Soc., 24 (2004) 3295-3302.https://doi.org/10.1016/j.jeurceramsoc.2003.10.014

[31] Z. Z. Ali, F. J. Al-Hasani, Evaluation of surface roughness of some biomedical titanium alloys by pack cementation coating, Key Eng. Mater., 886 (2021) 189-202.https://doi.org/10.4028/www.scientific.net/KEM.886.189